# High Pressure Softening of the *out-of-plane* $A_{2u}$(TO) Mode of *h*-BN Induced by Dynamical Buckling

A. Segura,[†] R. Cuscó,[‡] T. Taniguchi,[¶] K. Watanabe,[¶] G. Cassabois,[§] B. Gil,[§] and L. Artús[‡]

† *Departamento de Física Aplicada-ICMUV, Malta-Consolider Team, Universitat de València, Burjassot, Spain.*

‡*Institut Jaume Almera (ICTJA-CSIC), Consejo Superior de Investigaciones Científicas, 08028 Barcelona, Spain.*

¶*National Institute for Materials Science,1-1 Namiki, Tsukuba, 305-0044, Japan.*

§*Laboratoire Charles Coulomb (L2C), UMR 5221 CNRS-Université de Montpellier, F-34095, Montpellier, France.*

**Abstract**

We investigate the highly anisotropic behavior of the *in-plane* and *out-of-plane* infrared-active phonons of *h*-BN by means of infrared reflectivity and absorption measurements under high pressure. Infrared reflectivity spectra at normal incidence on high quality single crystals show strict fulfillment of selection rules and an unusually long $E_{1u}$(TO) phonon lifetime. Accurate values of the dielectric constants at ambient pressure $\varepsilon_0^{\perp} = 6.96$, $\varepsilon_\infty^{\perp} = 4.95$, $\varepsilon_0^{\parallel} = 3.37$, and $\varepsilon_\infty^{\parallel} = 2.84$ have been determined from fits to the reflectivity spectra. The *out-of-plane* $A_{2u}$ phonon reflectivity band is revealed in measurements on an inclined facet, and absorption measurements at an incidence angle of 30° allow us to observe both the $A_{2u}$ TO and LO modes. Pressure coefficients and Grüneisen parameters for all infrared-active modes are determined and compared with *ab-initio* calculations. While Grüneisen parameters are generally small in this layered crystal, the $A_{2u}$(TO) displays an exceptionally large and negative Grüneisen parameter that results in a widening of the type I hyperbolic region with increasing pressure. The softening of the $A_{2u}$(TO) mode is induced by a dynamical buckling of the flat honeycomb layers.

# Introduction

Hexagonal boron nitride ($h$-BN) is attracting a great deal of attention in the emerging field of two-dimensional atomic crystals and van der Waals heterostructures.[1] Given its atomically smooth surface that is relatively free of dangling bonds and its lattice constant similar to graphene,[2] $h$-BN gained prominence as an excellent substrate for graphene electronics[3] and has become an essential building block for dielectric interfaces in atomically thin van der Waals stacked heterostructures.[4] The promising applications of $h$-BN have spurred the research of its basic physical properties. It has been recently shown that $h$-BN is an indirect bandgap semiconductor[5] that displays a rich structure of phonon-assisted emission owing to its distinctive electronic structure.[6]

On the other hand, the extreme optical anisotropy of $h$-BN[7] results in optical hyperbolic behavior[8] in the mid-infrared (MIR), where the permittivities along orthogonal axes have opposite signs. This makes $h$-BN a low-loss natural hyperbolic material with great potential to confine and control slow-light phonon-polariton modes at the nanoscale,[9–11] which opens exciting avenues for nanophotonic applications of novel optical phenomena, such as subdiffractional focusing and multi-mode waveguiding.[9] $h$-BN is particularly well suited for these applications because of the low optical losses of phonon polaritons, the strong and broad phonon resonances in the technologically relevant MIR spectral region, and the concurrence of Type I and Type II hyperbolic response in the same material. Subdiffractional Type I and Type II hyperbolic polaritons confined in all three dimensions with high quality factors have been recently reported in $h$-BN.[10]

Phonon-polariton propagation length is essentially limited by the phonon-polariton lifetime, which is on the order of the optical phonon lifetimes.[12] $h$-BN being a centrosymmetrical crystal, its optically active phonons are either Raman or infrared (IR) active. The Raman-active optical phonons ($E_{2g}$ symmetry) have been investigated in detail in high-quality single crystals by means of Raman scattering.[13,14] Quite recently, the availability of high-quality isotopically purified $h$-BN crystals has allowed the demonstration of a threefold increase of phonon-

polariton lifetime in isotopically pure samples.[15] This milestone, together with the outstanding applications of boron 10 in solid-state *h*-BN neutron detectors,[16] have newly triggered a number of basic research works on isotopic effects on the phonons of *h*-BN.[17–20]

Given the topical interest of IR-active modes in phonon-polariton applications, early studies of the IR-active modes (*in-plane* $E_{1u}$ and *out-of-plane* $A_{2u}$ modes) performed on pyrolytic *h*-BN are highly cited.[21] However, in those studies, the IR reflectivity spectra exhibit two reststrahlen bands for each direction of polarization ($E \parallel c$ or $E \perp c$).[21] This clearly indicates the polycrystalline nature of the pyrolytic samples used, which probably had a poor crystallinity and a large variation of the basal plane orientations. As a result, selection rules for $E \parallel c$ and $E \perp c$ polarizations were not fulfilled, and the dielectric function anisotropy was largely underestimated.[7] Considering the central role of the IR-active phonons in limiting the phonon-polariton propagation length and the availability today of high-quality *h*-BN single crystals, we have revisited the polar phonons and dielectric properties of *h*-BN and we study the anisotropic pressure dependence of the *in-plane* and *out-of-plane* IR-active modes up to 10 GPa. Accurate measurements of the IR-active phonons of *h*-BN are of great interest to assess the ultimate performance of phonon-polariton devices, as phonon-polariton lifetimes are usually estimated from Raman measurements of the $E_{2g}$ mode,[15] while the polaritons actually couple to the IR modes.

Early *ab-initio* calculations predicted a strongly anisotropic compression of the lamellar *h*-BN crystal.[22] Hydrostatic pressure mainly reduces the distance between the hexagonal layers and has relative little effect on the bond length in the layers. As a result, the optical modes with polarization vectors within the plane exhibit small, positive Grüneisen parameters, whereas the TO modes between 600 and 800 $cm^{-1}$ and polarization vectors perpendicular to the basal plane have negative Grüneisen parameters.[22] The $A_{2u}$(TO) modes induce a dynamical buckling of the flat honeycomb sheets which becomes easier under compression and has been proposed as a lattice instability that can lead to a phase transition in analogy with the graphene to diamond transition.[22] Detailed x-ray scattering experiments have revealed the pathway for the formation of $sp^3$ bonding in cold-compressed *h*-BN, which involves the direct bonding of atoms in the *c*-

axis direction and a buckling deformation of the hexagonal layers.[23] More recently, an allotropic structure of carbon (Z-carbon) has been identified in cold-compressed graphite which results from a combination of sliding an buckling of the graphene sheets.[24] Thus, buckling mechanisms play an ubiquitous role in the stability of lamellar crystals. In this work, we use IR measurements under oblique incidence to gain experimental access to the *out-of-plane* polarized $A_{2u}$ mode. This allows us to investigate the impact of the buckling mechanism on the pressure dependence of this mode, which is expected to be enhanced by polar interactions in the *h*-BN lattice.

## Experimental and Modeling Methods

High quality *h*-BN single crystals were synthesized at 4.5 GPa and 1500 °C using barium boron nitride as a solvent in a modified belt-type high-pressure and high-temperature apparatus.[25] Samples of thickness ranging from 5 to 500 $\mu$m were cleaved from *h*-BN single crystalline platelets.

Optical measurements to determine the refractive index dispersion were performed in the near-infrared (NIR), visible, and ultraviolet (UV) range using a home-made microscopic bench with deuterium and halogen lamps, reflecting objectives, and several multichannel spectrometers to cover the 15000–45000 $cm^{-1}$ spectral range. Optical measurements in the MIR range (450–4000 $cm^{-1}$) were performed by means of Fourier Transform Infrared Spectroscopy (FTIR) using an Interspectrum TEO-400 Michelson interferometer module coupled to a non-commercial all-reflecting microscope optical bench and a 22-$\mu$m HgCdTe detector.[26]

Measurements under pressure were performed in a membrane diamond anvil cell (DAC)[27] equipped with type-IIac diamond anvils. KBr was used as pressure transmitting medium (PTM). Pressure was determined using the ruby linear scale.[28,29] Methanol-ethanol-water (16:3:1) and KBr were used as PTM in the NIR-visible and MIR ranges, respectively. While the first PTM is known to be hydrostatic in the whole pressure range explored here,[30] it has been reported that KBr can give rise to non-hydrostatic tensions.[31] We have checked the pressure distribution in

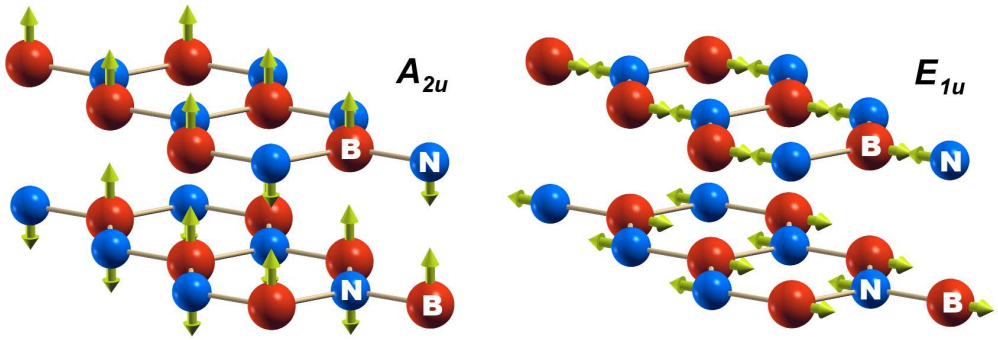


Figure 1: Atomic motions of the *out-of-plane* ($A_{2u}$) and *in-plane* ($E_{1u}$) infrared-active modes of $h$-BN. The arrows represent the eigenvectors obtained from *ab-initio* calculations. Atomic species are indicated on the atoms of the unit cell.

the KBr charged DAC chamber by using several ruby bills. With the hydrostaticity criteria defined in Ref. 30, KBr shows a better behavior than silicone oil up to 10 GPa. Normalized transmittance and reflectance spectra were obtained by dividing the spectra by a reference spectrum measured through the empty DAC.

Density functional theory (DFT) calculations were performed in the local density approximation (LDA) using the ABINIT code.[32] Troulliers-Martins pseudopotentials in the Teter-Pade parametrization were employed. Integration over the Brillouin zone was carried out using a $9 \times 9 \times 4$ Monkhorst-Pack grid, with an energy cut-off of 70 Hartree. The LDA approach yields a good description of $h$-BN phonon frequencies and their pressure dependence. As a further test to check the applicability of the present LDA calculations to model the lattice dynamics in $h$-BN, we have calculated the bulk modulus. We find $B = -V_0(\partial P/\partial V) = 26.6$ GPa, in excellent agreement with the value of 25.6 determined by inelastic x-ray scattering.[33]

# Results and discussion

## *In-plane* and *out-of-plane* infrared-active phonons

The atomic motions of $A_{2u}$ and $E_{1u}$ IR-active phonons of $h$-BN are illustrated in Figure 1. Both modes are odd under inversion symmetry, and there is a net displacement between anions

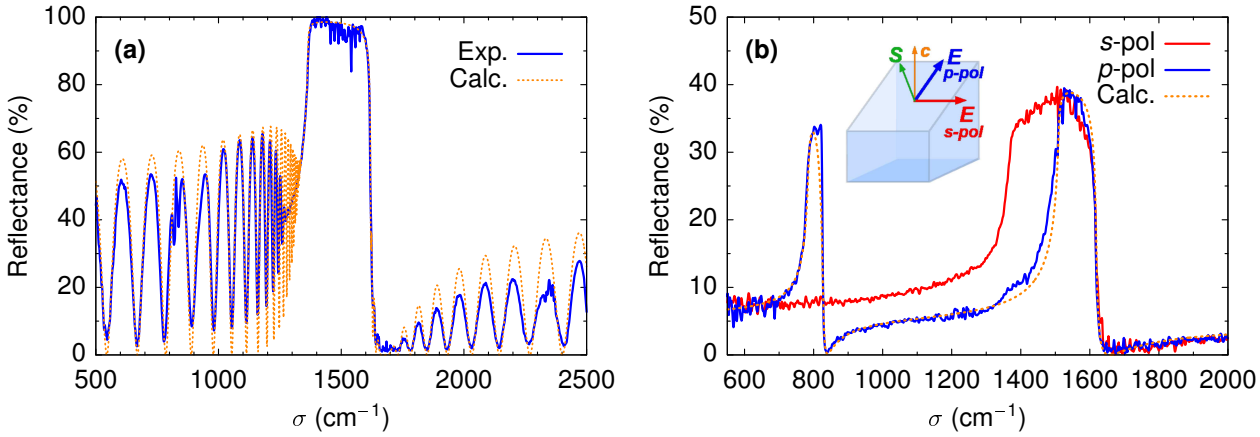


Figure 2: (a) Reflectance spectrum at normal incidence with $E \perp c$. The dotted line is the reflectance spectrum calculated by fitting the model dielectric function [Eq. (1)] taking into account the back side reflection. (b) Reflectance spectra at normal incidence on a specular facet at an angle $\theta \sim 38°$ relative to the $c$ face. The blue and red solid lines are the spectra obtained in $p$- and $s$-polarization. The dotted line is the reflectance spectrum calculated by fitting the model dielectric function given by Eq. (2) with $\theta = 38°$.

and cations in the unit cell that induces a dipole moment along the $c$ direction or along an *in-plane* direction, respectively. The $E_{1u}$ mode involves *in-plane* vibrations of boron and nitrogen atoms against each other, and therefore it probes the strong covalent bond, which yields a high phonon frequency. In the $A_{2u}$ mode, the vibrations of boron against nitrogen take place between atoms in adjacent layers and are along the $c$ direction. The atomic motions involve a dynamical buckling of the flat honeycomb layers, so that, unlike the $E_{1u}$ mode, the covalent boron-nitrogen bonds of the honeycomb structure do not lie strictly in the basal plane. This dynamical deformation introduces a component of covalent bond stretching in the restoring force along the $c$ direction, which results in the $A_{2u}$ modes lying in an intermediate frequency range. The buckling of the sheets tends to release the *in-plane* strain under compression, and, as we shall see later, it lends the $A_{2u}$ phonon its singular pressure dependence.

## Dielectric properties at ambient pressure

Figure 2 displays the reflectance spectra in the MIR range at normal incidence on a $c$ face with $E \perp c$ (a) and on a sample with a specular facet at an angle $\theta \sim 38°$ for $s$- and $p$-polarization

(b). In contrast to the results reported in Ref. 21, a single reststrahlen region associated with the $E_{1u}$ phonon is observed at normal incidence on a $c$ face, in agreement with symmetry selection rules. Reflectance measurements at normal incidence performed on an inclined facet exhibit an intense additional band at lower wavevectors in $p$-polarization which is completely extinguished in $s$-polarization. The $c$ component of the electric field in $p$-polarization enables the coupling to the $A_{2u}$ phonon, which involves atomic motions along the $c$ direction. The reflectance spectrum is modeled by taking into account the contribution of the polar modes to the dielectric function

$$\varepsilon_i(\sigma) = \varepsilon_\infty^i + (\varepsilon_0^i - \varepsilon_\infty^i)\frac{\sigma_i^2}{\sigma_i^2 - \sigma^2 - i\Gamma_i\sigma}, \tag{1}$$

where $i = \parallel, \perp$ denotes light polarization parallel or perpendicular to the $c$ axis, $\varepsilon_0^i$ is the static dielectric constant, $\varepsilon_\infty^i$ is the electronic contribution, and $\sigma_i$ and $\Gamma_i$ are the frequency and damping of the transverse polar optical mode that couples to light [$E_{1u}$(TO) and $A_{2u}$(TO) for $i = \perp$ and $\parallel$, respectively].

The sample reflectance at normal incidence can be calculated using Eq. (1) for $\varepsilon_\perp(\sigma)$ in the model of a dielectric slab between two different media developed by Heavens.[34] A fit to the reflectivity spectrum for polarization perpendicular to the $c$ axis yields $\varepsilon_0^\perp = 6.96$ and $\varepsilon_\infty^\perp = 4.95$, in good agreement with the results reported by Geick *et al.* in pyrolytic $h$-BN.[21] However, we find a substantially smaller damping parameter $\Gamma_\perp = 4$ cm$^{-1}$ compared to the value of $\Gamma_\perp = 29$ cm$^{-1}$ reported in Ref. 21. Such a small value of $\Gamma_\perp$ indicates an unusually long lifetime of the $E_{1u}$ phonon mode, much longer than that of the Raman-active $E_{2g}$ mode.[18] A similar situation is found in graphite, where the line widths for the IR-active $E_{1u}$ and Raman-active $E_{2g}$ phonons were reported to be 4.2 and 12.9 cm$^{-1}$, respectively.[35] This implies that the ultimate phonon-polariton propagation length in $h$-BN may be longer than the expected values that are usually estimated from the Raman-active $E_{2g}$ phonon lifetime.[15] The periodic oscillations in the reflectivity that are clearly visible in Fig. 2 (a) arise from multiple reflections in the $d = 13.5$-$\mu$m thick sample. Very accurate values of the refractive index $n_\perp(\sigma)$ at the reflectance minima can be obtained from the interference condition.[7]

Coupling to the $c$-polarized $A_{2u}$ mode occurs in normal-incidence reflectance measurements on an inclined face in $p$-polarization on account of the $c$ component of the electric field [see inset of Fig. 2(b)]. Then, the reflectance spectra displays a strong resonance in the frequency range of the $A_{2u}$ phonons. The $s$- and $p$-polarization reflectance spectra are shown in Fig. 2(b). They strictly fulfill the selection rules, showing only the reststrahlen band of $E_{1u}$ phonons in $s$-polarization and both $E_{1u}$ and $A_{2u}$ reststrahlen bands in $p$-polarization. The normal-incidence reflectance in the $p$-polarization configuration on the inclined face (at an angle $\theta$ to the $c$ axis) can be calculated from the effective dielectric function[36]

$$\frac{1}{\varepsilon_\theta(\sigma)} = \frac{\cos^2\theta}{\varepsilon_\perp(\sigma)} + \frac{\sin^2\theta}{\varepsilon_\parallel(\sigma)}. \tag{2}$$

Using the model dielectric function given by Eqs. (1) and (2), a good fit to the experimental reflectance spectrum is obtained for $\theta = 38°$, $\sigma_\parallel[A_{2u}(TO)] = 767$ cm$^{-1}$, $\varepsilon_\infty^\parallel = 2.84$, and $\varepsilon_0^\parallel = 3.37$. These values of the dielectric constants are significantly lower than those reported in pyrolytic samples.[21] Note that the values of the dielectric constants can be obtained to a high accuracy by reproducing the frequencies at which the interference maxima and minima are observed in the reflectance spectra. Therefore, the precision of the measurement is determined by the high resolution of Fourier Transform IR spectroscopy. Our results are in good agreement with theoretical predictions[37,38] and truly reflect the high anisotropy of the $h$-BN crystal, which was reported to exhibit the highest birefringence in a bulk crystal through the MIR to UV range.[7] Recent determinations of the dielectric tensor in nanometer-thin layers of $h$-BN by near-field imaging have also revealed highly anisotropic optical responses in the visible region at 632.8 nm.[39]

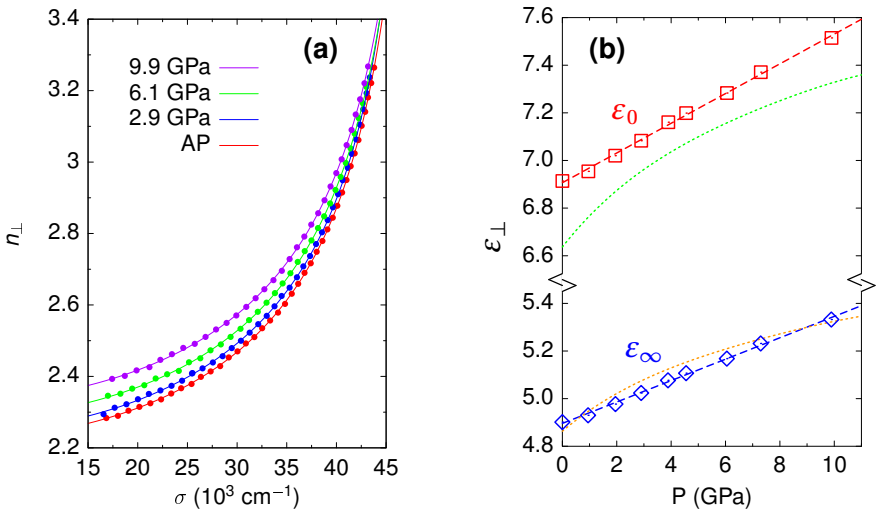


Figure 3: (a) Experimental values of the refractive index for polarization perpendicular to the $c$ axis obtained from the interference pattern of the transmission spectra (filled dots) at several pressures from ambient pressure (AP) up to 9.9 GPa. Solid lines are fits of a modified Phillips-van Vechten model with an additional excitonic term. (b) Pressure dependence of the static (squares) and electronic (diamonds) dielectric constants for polarization perpendicular to the $c$ axis extracted from model fits to the refractive index data. Dashed lines are linear fits to the data. Dotted lines are theoretical results obtained from DFT calculations.

## Dielectric properties under high pressure

### Pressure dependence of the dielectric constant

The pressure dependence of the refractive index for light polarization perpendicular to the $c$-axis, $n_\perp$, was determined from the pressure evolution of the interference maxima of the transmittance spectra. Once the interference order $K$ and the sample thickness $d$ are unambiguously determined at ambient pressure, the refractive index at a given pressure $P$ and wavelength $\lambda_K(P)$ is obtained from the constructive interference condition $2n_\perp(P)d(P) = K\lambda_K(P)$, assuming that the sample thickness decreases with $P$ according to the pressure dependence of the $c$ lattice parameter. The latter was evaluated from DFT calculations, which yield results in excellent agreement with x-ray diffraction data.[40]

The values of the refractive index for polarization perpendicular to the $c$ axis determined from the interference maxima in the NIR-UV region are shown in Fig. 3(a) for several pressures

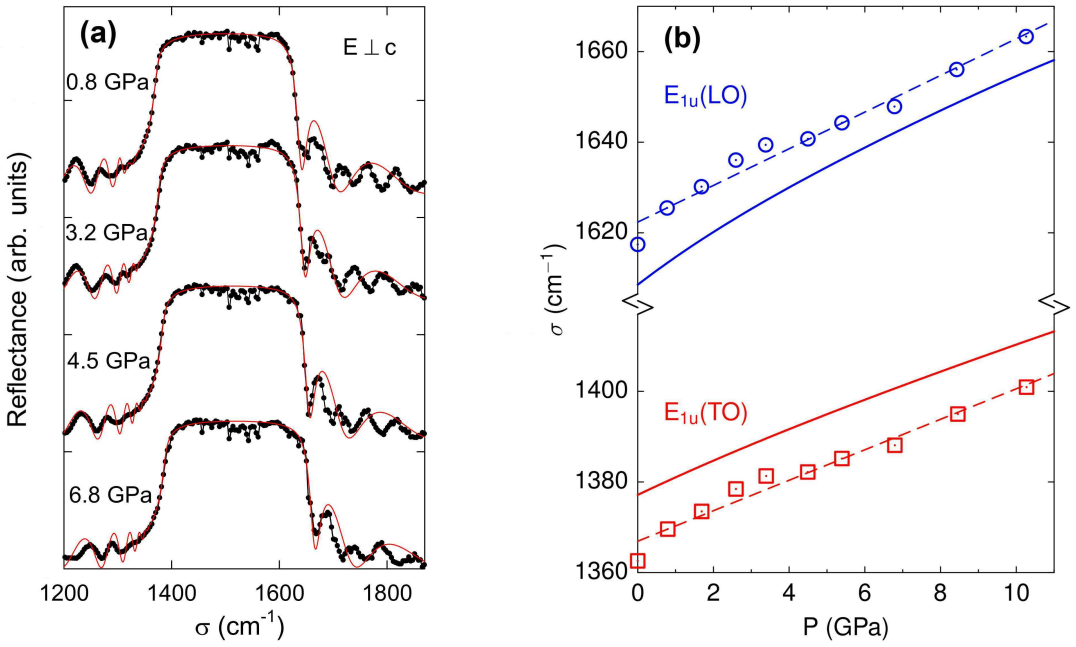


Figure 4: (a) Reflectance spectra at normal incidence with $E \perp c$ for increasing pressure. The red line is the model dielectric function fitted to the reflectance spectra. (b) $E_{1u}$(LO) and $E_{1u}$(TO) phonon frequencies as a function of pressure determined from the reflectance spectra (symbols) and theoretical values obtained from density functional calculations (solid lines). Dashed lines are linear fits to the data.

up to 10 GPa, beyond which the hexagonal phase becomes unstable. A phase transition to a wurtzite phase at ~ 14 GPa has been observed by means of inelastic x-ray scattering experiments.[23] Assuming a linear increase of the Penn gap and the exciton energies with pressure, fitting the modified Phillips-van Vechten model (see Ref. 7) to the refractive index data yields the solid lines displayed in Fig. 3(a), with linear pressure coefficients of $27 \pm 2$ and $10 \pm 1$ meV GPa$^{-1}$ for the Penn gap and the exciton energies, respectively. This different pressure dependence is consistent with the electronic structure of $h$-BN, where the exciton absorption is associated with transitions between states with $\pi$-bond orbital character whereas the Penn gap is associated with states of $\sigma$-bond orbital character,[38] the coupling potential dependence on pressure being much larger for $\sigma$ bonds. The *in-plane* refractive index of $n_o = 2.31$ at 632.8 nm that was determined in nanometer-thin $h$-BN flakes by near-field imaging of the waveguide modes[39] is in very good agreement with the refractive index dispersion at ambient pressure

**Table 1: Values of phonon frequency at ambient pressure, pressure coefficient and Grüneisen parameter for the polar phonons of $h$-BN extracted from fits to the infrared reflectance measurements compared to results of DFT calculations. The experimental values of the phonon frequency at ambient pressure and the pressure coefficient are obtained from linear fits to the data shown in Fig. 4 (b)**

| | $\sigma$ (cm$^{-1}$) | | $\frac{d\sigma}{dP}$ (cm$^{-1}$ GPa$^{-1}$) | | $\gamma$ | |
|---|---|---|---|---|---|---|
| | Experiment | Theory | Experiment | Theory | Experiment | Theory |
| $E_{1u}$(TO) | 1365 | 1377 | 3.4 | 4.1 | 0.090 | 0.078 |
| $E_{1u}$(LO) | 1623 | 1609 | 4.0 | 6.7 | 0.090 | 0.109 |
| $A_{2u}$(TO) | 767 | 750 | −8.3 | −12.1 | −0.39 | −0.42 |
| $A_{2u}$(LO) | 825 | 818 | 0.88 | 0.59 | 0.038 | 0.019 |

reported in Fig. 3(a). Figure 3(b) shows the pressure dependence of the dielectric constant determined from the model fit to the refractive index data. Dashed lines are linear fits to the data, which yield a pressure coefficient of $0.047 \pm 0.002$ GPa$^{-1}$ for the electronic dielectric constant. A good agreement is found with the theoretical dielectric constant derived from DFT calculations (dotted lines).

### Pressure dependence of the *in-plane* $E_{1u}$ phonons

Reflectance measurements were recorded in DAC at pressures up to 10 GPa. Representative spectra are displayed in Fig. 4(a). The interference oscillations are strongly reduced because of the small difference of refractive indices at the diamond-sample and sample-KBr interfaces. The interference fringe pattern is determined by the sample refractive index only when its value is large enough to provide a large contrast with the PTM (KBr). In the high-frequency region of the spectra, the refractive index of $h$-BN is very close to that of KBr, and the interference pattern corresponds to the diamond/sample+KBr/diamond Fabry-Perot cavity. This explains the discrepancy between the observed reflectivity oscillations and the calculated interference pattern, which was obtained from the model of a dielectric slab between two different media[34] by considering the values of $\varepsilon_{\perp}(\sigma)$ and thickness corresponding to the $h$-BN sample.

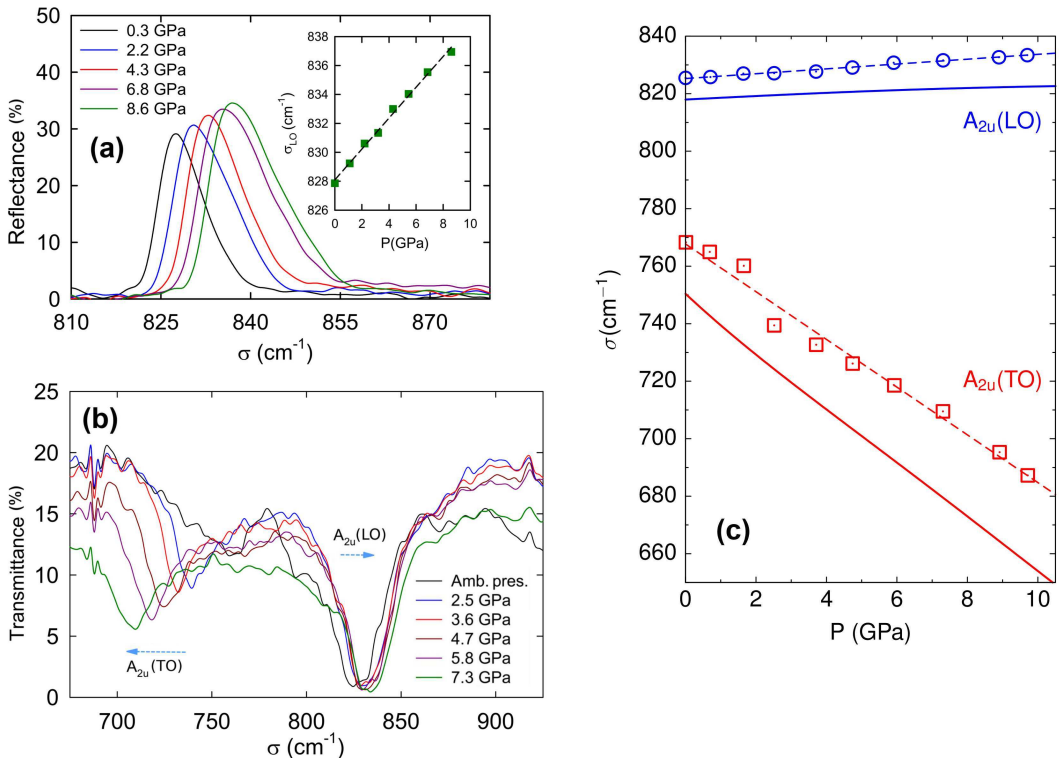


Figure 5: (a) Unpolarized reflection spectra at an incidence angle of $\theta \sim 30°$ for increasing pressures up to 8.6 GPa. The inset shows the blueshift of the reflection peak. (b) Transmittance spectra with $\theta \sim 30°$ in $p$-polarization in the spectral range of the $A_{2u}$ phonons for increasing pressures up to 7.3 GPa. (c) Pressure dependence of the $A_{2u}$ modes obtained from the transmittance spectra (symbols). Dashed lines are linear fits to the data. The solid lines correspond to values obtained from DFT calculations.

The reststrahlen band associated with the $E_{1u}$ modes shifts to higher frequencies with increasing pressure. DFT calculations yield $\varepsilon_0^{\perp}/\varepsilon_\infty^{\perp}$ ratios that change by less than 1% in this pressure range, indicating that *in-plane* polarizability is virtually independent of pressure. Indeed, considering the frequencies at half maximum of the reststrahlen band as rough estimations of the transverse-optic (TO) and longitudinal-optic (LO) phonon frequencies, we find that the LO/TO frequency ratio squared remains constant within the experimental error up to 10 GPa. With the assumption of a constant $\varepsilon_0^{\perp}/\varepsilon_\infty^{\perp}$ ratio, the reflectance spectra was calculated and fitted to the experimental data. The calculated reflectance, displayed as red lines in Fig. 4(a), nicely reproduces the interference oscillations below the TO frequency as well as the sharp reflectance minimum near the LO frequency, thus confirming the adequacy of the model assumptions.

The pressure dependence of the fitted phonon frequencies are plotted in Fig. 4(b). Linear fits to these data yield the pressure coefficients and Grüneisen parameters for these modes that are listed in Table 1 and compared to the theoretical values calculated at ambient pressure. The differences between experimental and theoretical pressure coefficients are essentially due to the fact that the theoretical values are calculated at ambient pressure and account for the non-linearity of the pressure dependence, which reflects the strongly nonlinear behavior of *h*-BN equation of state at very low pressures. In contrast, only an average linear coefficient can be determined from the experimental data, given the pressure range of a DAC and the precision of the ruby scale in the low pressure range. The pressure dependence of the $E_{1u}$ phonon frequencies obtained from DFT calculations is displayed in Fig. 4(b) as solid lines. Experimental and theoretical values of the $E_{1u}$ frequencies agree to within 1%, and their pressure dependence is accurately predicted by the calculations. The pressure coefficient we obtain for the *in-plane* $E_{1u}$ IR active mode is close to the value of 4.3 $cm^{-1}$/GPa previously reported for the *in-plane* $E_{2g}^{high}$ Raman active mode.[41]

**Pressure dependence of the *out-of-plane* $A_{2u}$ phonons**

When reflectivity measurements are carried out at a small angle relative to normal incidence in *p*-polarization configuration, an additional reflection peak appears near the $A_{2u}$(LO) frequency. Figure 5(a) shows reflection spectra at $\theta \sim 30°$ for non-polarized light at different pressures in the $A_{2u}$(LO) spectral range. This reflection peaks exhibits a linear blueshift with increasing pressure that is much smaller than the one observed for the $E_{2u}$ phonons. No structure associated with the $A_{2u}$ (TO) phonon is detected in the reflection spectra. This is consistent with simulations of the reflection spectra for relatively small incidence angles using the reflectance equations of a dielectric slab.[34,42] The reflectance peak corresponds to the small interval of frequencies in which the dielectric constant for polarization parallel to the *c*-axis becomes negative, i.e. the spectral region where the material becomes hyperbolic (see Fig. 6 below).

To study in more detail the *out-of-plane* $A_{2u}$ phonons, transmission measurements were

carried out at an incidence angle of $\theta \sim 30^\circ$. In $p$-polarization configuration, which enables the propagation of the extraordinary ray, two absorption peaks are detected in the $A_{2u}$ spectral range. The spectra at oblique incidence are shown in Fig. 5(b) for pressures up to 7.3 GPa. The peak centered at $\sim 845$ cm$^{-1}$ blueshifts as pressure increases, with a pressure coefficient of $0.88 \pm 0.04$ cm$^{-1}$GPa$^{-1}$. Both the frequency at ambient pressure and the pressure coefficient are close to those measured on the reflection peak. Thus, we ascribe this absorption peak to the transmission counterpart of the reflection peak associated with the $A_{2u}$(LO) phonon. A second peak develops at lower frequencies as frequency increases and redshifts with a negative and much larger pressure coefficient ($-8.3 \pm 0.4$cm$^{-1}$GPa$^{-1}$). This peak is attributed to the $A_{2u}$(TO) phonon. The pressure dependence of these peaks is plotted in Fig. 5(c), where the experimental points are compared with the predictions of our DFT calculations. The pressure coefficients and Grüneisen parameters for these phonon modes are extracted from linear fits to the data, and are listed in Table 1. The values derived from DFT calculations for the pressure coefficients and Grüneisen parameters are in fair agreement with the measurements. Notably, the large and negative pressure coefficient of the $A_{2u}$(TO) mode is correctly predicted by the theory. Earlier lattice dynamics calculations based on the force-constant method already indicated that the TO modes with *out-of-plane* polarization at intermediate frequencies (600–800 cm$^{-1}$) have negative Grüneisen parameters.[22] These modes involve a dynamical buckling of the hexagonal layers (see Fig. 1) that becomes easier under pressure, and it has been suggested that they may be associated with a destabilization of the layered $h$-BN phase under compression,[22] leading to a pressure-induced phase transition to the wurtzite phase. A similar buckling instability has been proposed to drive the pressure-induced transition of graphite to the Z-carbon structure.[24] In $h$-BN, the buckling instability is probably enhanced by the polar character of the lattice, and gives rise to a substantial softening of the $A_{2u}$(TO) phonon at high pressure. A rather large and negative Grüneisen parameter $\gamma \sim -0.8$ was calculated in Ref. 22 for the $A_{2u}$(TO) phonon at zone center. Our measurements yield a somewhat lower value of $\gamma = -0.39$, which is in good agreement with our DFT calculations.

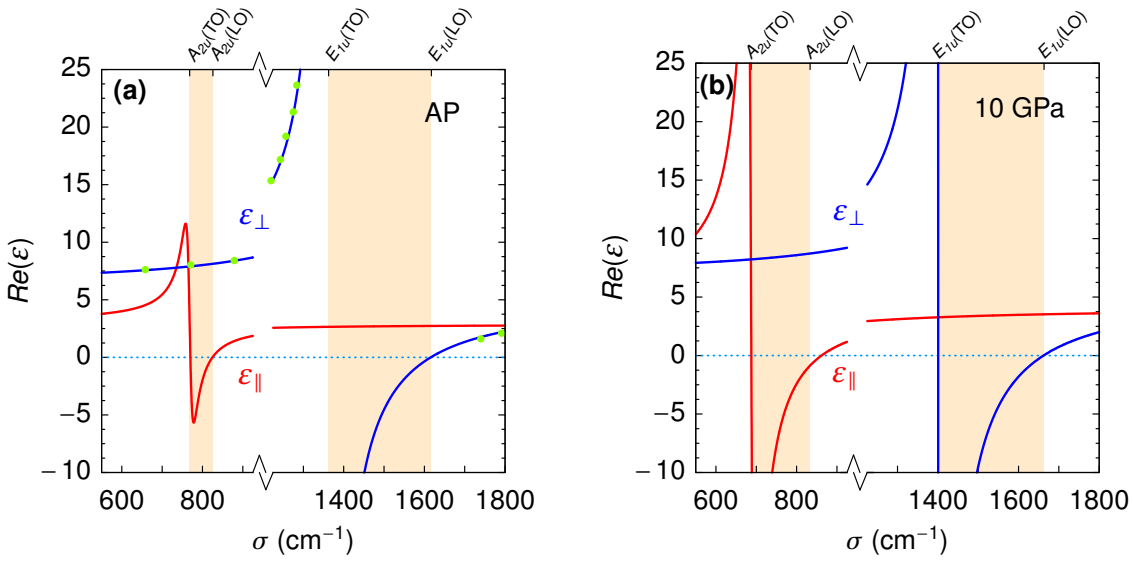


Figure 6: (a) Real part of the dielectric function for polarization perpendicular (blue line) or parallel (red line) to the $c$ axis around the reststrahlen bands of $h$-BN at ambient pressure. The green dots are experimental values determined from the interference pattern in IR-transmission measurements. (b) Idem at 10 GPa.

**Type I and Type II hyperbolicity regions**

On account of its strong anisotropy, $h$-BN features both type I and type II hyperbolic response associated with the low- and high-frequency reststrahlen bands (LR, HR), respectively, where the *in-plane* permittivity is positive (negative) in the LR (HR) bands and the *out-of-plane* permittivity is opposite in sign. Distinct series of type I and type II hyperbolic polaritons have been observed in $h$-BN.[10]

Using the knowledge of $h$-BN dielectric properties gained from our IR study, a precise description of the dielectric constant in the LR and HR regions can be given. Figure 6 displays a plot of the *in-plane* ($\varepsilon_\perp$) and *out-of-plane* ($\varepsilon_\parallel$) permittivities around the LR and HR bands at ambient pressure and at 10 GPa. A narrow, shallow type I hyperbolic region develops in the LR band. With increasing pressure, the LR band widens substantially and the *out-of-plane* permittivity becomes more negative. In the HR band, the difference between *in-plane* and *out-of-plane* permittivities is higher, and both this difference and the hyperbolic region increase with pressure.

## Conclusions

The *in-plane* and *out-of-plane* IR-active phonons of $h$-BN have been studied on high quality single crystals by means of normal- and off-normal-incidence IR reflectance and transmission measurements, and their behavior under high pressure has been investigated. Unlike early works on preferentially oriented pyrolytic $h$-BN samples, our measurements on high quality $h$-BN single crystals fully reveal the strong anisotropy of the material, with strict adherence to selection rules. An unusually long lifetime of the $E_{1u}$(TO) phonon is revealed by the model fit to the reflectance spectra. Pressure coefficients and Grüneisen parameters have been determined for all IR-active modes. Grüneisen parameters are generally small because compression decreases mainly the interlayer distance and has only a minor effect on the *in-plane* lattice constant. However, the $A_{2u}$(TO) phonon exhibits an unusually large and negative Grüneisen parameter. The substantial softening of the $A_{2u}$(TO) phonon at high pressure is due to the dynamical buckling of the hexagonal layers associated with the atomic motions. As a result of the $A_{2u}$(TO) softening, the LR band considerably widens with increasing pressure and displays a notable increase of the magnitude of the negative *out-of-plane* permittivity in the type I hyperbolic region.

## Acknowledgements

This work has been supported by the Spanish MINECO/FEDER under Contracts No.MAT2015-71035-R and No. MAT2016-75586-C4-1-P. T. T. acknowledges support from the Elemental Strategy Initiative conducted by the MEXT, Japan and JSPS KAKENHI Grant Number JP15K21722. B. G. acknowledges support from the Government of the Russian Federation, contract #14.W03.31.0011 at Ioffe Institute.

# References


(1) Geim, A. K.; Grigorieva, I. V. Van der Waals heterostructures. *Nature* **2013**, *499*, 419–425.

(2) Xue, J.; Sanchez-Yamagishi, J.; Bulmash, D.; Jacquod, P.; Deshpande, A.; Watanabe, K.; Taniguchi, T.; Jarillo-Herrero, P.; LeRoy, B. J. Scanning Tunnelling Microscopy and Spectroscopy of Ultra-Flat Graphene on Hexagonal Boron Nitride. *Nature Mater.* **2011**, *10*, 282–285.

(3) Dean, C. R.; Young, A. F.; Meric, I.; Lee, C.; Wang, L.; Sorgenfrei, S.; Watanabe, K.; Taniguchi, T.; Kim, P.; Shepard, K. L. et al. Boron Nitride Substrates for High-Quality Graphene Electronics. *Nat. Nanotechnol.* **2010**, *5*, 722–726.

(4) Roy, T.; Tosun, M.; Kang, J. S.; Sachid, A. B.; Desai, S. B.; Hettick, M.; Hu, C. C.; Javey, A. Field-effect Transistors Built from All Two-Dimensional Material Components. *ACS Nano* **2014**, *8*, 6259–6264.

(5) Cassabois, G.; Valvin, P.; Gil, B. Hexagonal Boron Nitride is an Indirect Bandgap Semiconductor. *Nat. Photonics* **2016**, *10*, 262–266.

(6) Vuong, T. Q. P.; Cassabois, G.; Valvin, P.; Jacques, V.; Cuscó, R.; Artús, L.; Gil, B. Overtones of Interlayer Shear Modes in the Phonon-Assisted Phonon Spectrum of Hexagonal Boron Nitride. *Phys. Rev. B* **2017**, *95*, 045207.

(7) Segura, A.; Artús, L.; Cuscó, R.; Taniguchi, T.; Cassabois, G.; Gil, B. Natural Optical Anisotropy of h-BN: Highest Giant Birefringence in a Bulk Crystal through the Mid-Infrared to Ultraviolet Range. *Phys. Rev. Mater.* **2018**, *2*, 024001.

(8) Sun, J.; Litchinitser, N. M.; Zhou, J. Indefinite by Nature: From Ultraviolet to Terahertz. *ACS Photonics* **2014**, *1*, 293.

(9) Dai, S.; Ma, Q.; Andersen, T.; Mcleod, A. S.; Fei, Z.; Liu, M. K.; Wagner, M.; Watanabe, K.;

Taniguchi, T.; Thiemens, M. et al. Subdiffractional Focusing and Guiding of Polaritonic Rays in a Natural Hyperbolic Material. *Nat. Commun.* **2015**, *6*, 7963.

(10) Caldwell, J. D.; Kretinin, A. V.; Chen, Y.; Giannini, V.; Fogler, M. M.; Francescato, Y.; Ellis, C. T.; Tischler, J. G.; Woods, C. R.; Giles, A. J. et al. Sub-Diffractional Volume-Confined Polaritons in the Natural Hyperbolic Material Hexagonal Boron Nitride. *Nat. Commun.* **2014**, *5*, 5221.

(11) Yoxall, E.; Schnell, M.; Nikitin, A. Y.; Txoperena, O.; Woessner, A.; Lundeberg, M. B.; Casanova, F.; Hueso, L. E.; Koppens, F. H. L.; Hillenbrand, R. Direct Observation of Ultraslow Hyperbolic Polariton Propagation with Negative Phase Velocity. *Nat. Photonics* **2015**, *9*, 674.

(12) Low, T.; Chaves, A.; Caldwell, J. D.; Kumar, A.; Fang, N. X.; Avouris, P.; Heinz, T. F.; Guinea, F.; Martin-Moreno, L.; Koppens, F. Polaritons in Layered Two-Dimensional Materials. *Nat. Mater.* **2016**, *16*, 182–194.

(13) Reich, S.; Ferrari, A. C.; Arenal, R.; Loiseau, A.; Bello, I.; Robertson, J. Resonant Raman Scattering in Cubic and Hexagonal Boron Nitride. *Phys. Rev. B* **2005**, *71*, 205201.

(14) Cuscó, R.; Gil, B.; Cassabois, G.; Artús, L. Temperature Dependence of Raman-Active Phonons and Anharmonic Interactions in Layered Hexagonal BN. *Phys. Rev. B* **2016**, *94*, 155435.

(15) Giles, A. J.; Dai, S.; Vurgaftman, I.; Hoffman, T.; Liu, S.; Lindsay, L.; Ellis, C. T.; Assefa, N.; Chatzakis, I.; Reinecke, T. L. et al. Ultralow-Loss Polaritons in Isotopically Pure Boron Nitride. *Nat. Mater.* **2017**, *17*, 134–139.

(16) Maity, A.; Doan, T. C.; Li, J.; Lin, J. Y.; Jiang, H. X. Realization of Highly Efficient Hexagonal Boron Nitride Neutron Detectors. *Appl. Phys. Lett.* **2016**, *109*, 072101.

(17) Vuong, T. Q. P.; Liu, S.; van de Lee, A.; Cuscó, R.; Artús, L.; Michel, T.; Valvin, P.; Edgar, J. H.; Cassabois, G.; Gil, B. Isotope Engineering of van der Waals Interactions in Hexagonal Boron Nitride. *Nat. Mater.* **2018**, *17*, 152–158.

(18) Cuscó, R.; Artús, L.; Edgar, J. H.; Liu, S.; Cassabois, G.; Gil, B. Isotopic Effects on Phonon Anharmonicity in Layered van der Waals Crystals: Isotopically Pure Hexagonal Boron Nitride. *Phys. Rev. B* **2018**, *97*, 155435.

(19) Cuscó, R.; Edgar, J. H.; Liu, S.; Cassabois, G.; Gil, B.; Artús, L. Influence of Isotopic Substitution on the Anharmonicity of the Interlayer Shear Mode of h -BN. *Phys. Rev. B* **2019**, *99*, 085428.

(20) Cuscó, R.; Edgar, J.; Liu, S.; Cassabois, G.; Gil, B.; Artús, L. Effects of Isotopic Substitution on the Phonons of van der Waals Crystals: the Case of Hexagonal Boron Nitride. *J. Phys. D: Appl. Phys.* **2019**, *52*, 303001.

(21) Geick, R.; Perry, C. H.; Rupprecht, G. Normal Modes in Hexagonal Boron Nitride. *Phys. Rev.* **1966**, *146*, 543–547.

(22) Kern, G.; Kresse, G.; Hafner, J. Ab Initio Calculation of the Lattice Dynamics and Phase Diagram of Boron Nitride. *Phys. Rev. B* **1999**, *59*, 8551–8559.

(23) Meng, Y.; Mao, H.-k.; Eng, P. J.; Trainor, T. P.; Newville, M.; Hu, M. Y.; Kao, C.; Shu, J.; Hausermann, D.; Hemley, R. J. The Formation of $sp^3$ Bonding in Compressed BN. *Nat. Mater.* **2004**, *3*, 111–114.

(24) Amsler, M.; Flores-Livas, J. A.; Lehtovaara, L.; Balima, F.; Ghasemi, S. A.; Machon, D.; Pailhès, S.; Willand, A.; Caliste, D.; Botti, S. et al. Crystal Structure of Cold Compressed Graphite. *Phys. Rev. Lett.* **2012**, *108*.

(25) Taniguchi, T.; Watanabe, K. Synthesis of High-Purity Boron Nitride Single Crystals under High Pressure by Using Ba-BN Solvent. *J. Cryst. Growth* **2007**, *303*, 525–529.

(26) Panchal, V.; Segura, A.; Pellicer-Porres, J. Low-Cost Set-Up for Fourier-Transform Infrared Spectroscopy in Diamond Anvil Cell from 4000 to 400 $cm^{-1}$. *High Pressure Res.* **2011**, *31*, 445–453.

(27) Le Toullec, R.; Pinceaux, J.; Loubeyre, P. The Membrane Diamond Anvil Cell: A New Device for Generating Continuous Pressure and Temperature Variations. *High Pressure Res.* **1988**, *1*, 77–90.

(28) Mao, H. K.; Xu, J.; Bell, P. M. Calibration of the Ruby Pressure Gauge to 800 kbar under Quasi-Hydrostatic Conditions. *J. Geophys. Res.* **1986**, *91*, 4673.

(29) Chervin, J. C.; Canny, B.; Mancinelli, M. Ruby Spheres as Pressure Gauge for Optically Transparent High Pressure Cells. *High Pressure Res.* **2001**, *21*, 305–314.

(30) Klotz, S.; Chervin, J.-C.; Munsch, P.; Marchand, G. L. Hydrostatic Limits of 11 Pressure Transmitting Media. *J. Phys. D: Appl. Phys.* **2009**, *42*, 075413.

(31) Zhao, J.; Ross, N. L. Non-Hydrostatic Behavior of KBr as a Pressure Medium in Diamond Anvil Cells up to 5.63 GPa. *J. Phys.: Condens. Matter* **2015**, *27*, 185402 .

(32) ABINIT is a common project of the Université Catholique de Louvain, Corning Incorporated, and other contributors (http://www.abinit.org). X. Gonze,; Beuken, J.-M.; Caracas, R.; Detraux, F.; Fuchs, M.; Rignanese, G.-M.; Sindic, L.; Verstraete, M.; Zerah, G.; Jollet, F. et al. First-principles Computation of Material Properties: the ABINIT Software Project. *Comput. Mater. Sci.* **2002**, *25*, 478–492.

(33) Bosak, A.; Serrano, J.; Krisch, M.; Watanabe, K.; Taniguchi, T.; Kanda, H. Elasticity of Hexagonal Boron Nitride: Inelastic X-Ray Scattering Measurements. *Phys. Rev. B* **2006**, *73*, 041402(R).

(34) Heavens, O. S. *Optical Properties of Thin Solid Films*; Dover Publications: New York, 1991.

(35) Giura, P.; Bonini, N.; Creff, G.; Brubach, J. B.; Roy, P.; Lazzeri, M. Temperature Evolution of Infrared- and Raman-Active Phonons in Graphite. *Phys. Rev. B* **2012**, *86*, 121404(R).

(36) Lekner, J. Reflection and Refraction by Uniaxial Crystals. *J. Phys.: Condens. Matter* **1991**, *3*, 6121–6133.

(37) Ohba, N.; Miwa, K.; Nagasako, N.; Fukumoto, A. First-Principles Study on Structural, Dielectric, and Dynamical Properties for Three BN Polytypes. *Phys. Rev. B* **2001**, *63*, 115207.

(38) Arnaud, B.; Lebègue, S.; Rabiller, P.; Alouani, M. Huge Excitonic Effects in Layered Hexagonal Boron Nitride. *Phys. Rev. Lett.* **2006**, *96*, 026402.

(39) Hu, D.; Yang, X.; Li, C.; Liu, R.; Yao, Z.; Hu, H.; Corder, S. N. G.; Chen, J.; Sun, Z.; Liu, M. et al. Probing Optical Anisotropy of Nanometer-Thin van der Waals Microcrystals by Near-Field Imaging. *Nat. Commun.* **2017**, *8*, 1471.

(40) Solozhenko, V. L.; Will, G.; Elf, F. Isothermal Compression of Hexagonal Graphite-like Boron Nitride up to 12 GPa. *Solid State Comm.* **1995**, *96*, 1–3.

(41) Saha, S.; Muthu, D.; Golberg, D.; Tang, C.; Zhi, C.; Bando, Y.; Sood, A. Comparative High Pressure Raman Study of Boron Nitride Nanotubes and Hexagonal Boron Nitride. *Chem. Phys. Lett.* **2006**, *421*, 86–90.

(42) Tomlin, S. G. Optical Reflection and Transmission Formulae for Thin Films. *J. Phys. D: Appl. Phys.* **1968**, *1*, 1667.

Graphical TOC image.